実験動物を用いた内耳細胞治療研究へのアプローチ

神谷　和作・池田　勝久

Experimental Approaches to Inner Ear Cell Therapy Using Laboratory Animals

Kazusaku Kamiya and Katsuhisa Ikeda

(Juntendo University School of Medicine)

Recently, a number of clinical studies on cell therapy have been reported and used in clinical practice for several intractable diseases. Inner ear cell therapy for sensorineural hearing loss also has been studied using some laboratory animals, although to date reports on successful hearing recovery have been few.

Previously, we developed a novel rat model of acute sensorineural hearing loss due to fibrocyte dysfunction induced by a mitochondrial toxin and performed cell therapy with bone marrow mesenchymal stem cells (MSCs). In this study, we injected MSCs into the lateral semicircular canal; a number of these stem cells were then detected in the injured area in the lateral wall. Rats with transplanted MSCs in the lateral wall demonstrated a significantly higher hearing recovery ratio than the untreated controls. These results suggested that mesenchymal stem cell transplantation into the inner ear may be a promising therapy for patients with sensorineural hearing loss due to degeneration of cochlear fibrocytes.

In this article, we review studies on inner ear cell therapy using some laboratory animals including rodents such as mice and rats, and primates such as cynomologus monkeys (Macaca fascicularis).

Key words : inner ear, cell therapy, sensoryneural hearing loss, stem cell

はじめに

感音性難聴の原因は多岐にわたるが，近年の遺伝子改変動物開発技術の向上や多種のモデル動物の開発により多くの病態メカニズムが解明に近づいている．すべての先天性疾患の中でも頻度の高い遺伝性難聴においては，難聴家系や突然変異難聴マウスの遺伝子解析によって多くの遺伝性難聴原因遺伝子が同定されている．初期に発見された遺伝性難聴の原因の多くは内耳有毛細胞の変性または機能的・形態的異常であったため，多くの研究者が有毛細胞を中心に難聴の病態メカニズム解明に取り組んできた．哺乳類の有毛細胞は再生能力を持たないため遺伝子導入などによる有毛細胞再生の誘導も盛んに研究されてきた[1)2)]．その一方で内耳への細胞移植による有毛細胞の修復の試みも行われているが，特殊なリンパ液で満たされた内耳の構造的特徴から，聴力を保持しつつ標的部位に移植細胞を到達させ分化させることは容易ではない．そのため有毛細胞の修復には多種のモデル動物を用いた多くの検討実験が必要と考えられる．近年有毛細胞以外にも蝸牛線維細胞などの機能異常が単独で難聴病態の引き金となることも明らかとなっており，多様な治療戦略が求められている．幹細胞の損傷部への移動能力や組織環境（ニッシェ，niche）による分化誘導を十分に検討すれば細胞治療は内耳組織変性に対する治療にも応用可能と考えられる．著者らの報告では実験的に蝸牛線維細胞のみに傷害を与えたラットへ半規管外リンパ液を経由した細胞液還流法を用いることにより，損傷部の修復と聴力回復率を高めることに成功した[3)]．現在はヒト疾患に近い遺伝性難聴モデル動物への各種の幹細胞移植に取り組んでいる．また，サル類を用いた細胞移植アプローチの検討も今後応用性を高めるためには非常に重要であるため現在，カニクイザルによる検討を行っている．各種のモデル動物の特徴を考慮した細胞移植実験検討を

順天堂大学耳鼻咽喉科学教室

積み重ねることにより，将来的には有毛細胞も標的とした多様な難聴に対する聴力回復も不可能ではないと考えられる．本稿では各種実験動物を用いた内耳への細胞治療研究に関する知見について報告する．

内耳細胞治療実験に用いられる実験動物

外傷，騒音，感染，薬物障害，血流障害，加齢に起因する聴覚障害動物モデルは多く開発されており，細胞治療研究のための有用な実験モデルとして活用することができる．著者らはミトコンドリア阻害薬を用いて蝸牛線維細胞のみに損傷を与えるモデルラットを開発し，この細胞移植実験に成功している．しかしこのような実験的に内耳損傷を誘導した動物モデルがヒトと同等な内耳組織障害および機能的障害を忠実に再現しているかという点に関しては実証することは困難である．これに対し原因タンパク質がすでに特定されている遺伝子改変動物または突然変異動物はヒト遺伝性難聴の病態の多くが一致していると考えられる．細胞移植によりそのタンパク質が担う機能を回復させることができれば，幹細胞が正常に分化し失われていたタンパク質機能を取り戻した結果として聴力が回復したことを実証しやすい．有毛細胞の変性が顕著にみられるモデル動物としては，アッシャー症候群原因遺伝子（Pcdh15[4]，Cdh23[5]，Sans[6]，Harmonin[7]，MyosinVIIa[8]など）の突然変異動物あるいは遺伝子改変動物が，明白な表現型を持つため有毛細胞の研究に広く用いられている．これらの進行性の組織変性は重度であり有毛細胞の変性から連鎖的にラセン神経節細胞の消失へとつながる場合も多い．そのため細胞治療による細胞の生着・分化の検討は可能であるが聴力改善の検討は現段階で容易ではないと思われる．蝸牛線維細胞を標的とした場合，有毛細胞変性を伴わず蝸牛線維細胞のみに変性を持つ Brn4 欠損マウス[9]，Otospiralin 欠損マウス[10]が有効であると考えられる．これらの聴力改善の可能性は有毛細胞を標的とした細胞治療より格段に高いと思われる．ヒト遺伝性難聴でもっとも高頻度に出現するコネキシン26の遺伝子欠損マウスおよび優性阻害トランスジェニックマウス[11]は同遺伝子が蝸牛線維細胞および支持細胞に主に発現するため，著者らの行った骨髄間葉系幹細胞移植も有効であると考えられる．

蝸牛線維細胞を標的とした骨髄間葉系幹細胞移植

蝸牛ラセン靭帯およびラセン板縁を構成する蝸牛線維細胞はナトリウムポンプとギャップジャンクションによる蝸牛内イオンの能動輸送および受動輸送という単純な機能を担っている．しかしながら蝸牛線維細胞の傷害は複数の先天性および後天性難聴の主要因となることが示され，その重要性が近年示唆されている．とくにヒト非症候性難聴 DFN3 の原因因子 Brn4 の遺伝子欠損マウス[9]や otospiralin 欠損マウス[10]では蝸牛線維細胞の変性を主要因とした聴力低下が実証され，有毛細胞を含むコルチ器と同様に正常聴力を維持するうえで重要性の高い細胞群であることが明確に示された．また複数の加齢性難聴モデル動物においても蝸牛線維細胞の変性が他の細胞に先立ち開始することが報告されている[12)～14)]．また蝸牛線維細胞は単一細胞としての機能が単純であるにもかかわらず内耳機能における重要性が高いという点から，高度に分化した有毛細胞に比べて細胞治療が成功する可能性が格段に高いと考えられる．これらのことから蝸牛線維細胞は多種の感音難聴に対する新規治療法確立への重要な標的となりうると考えられる．著者らは薬剤

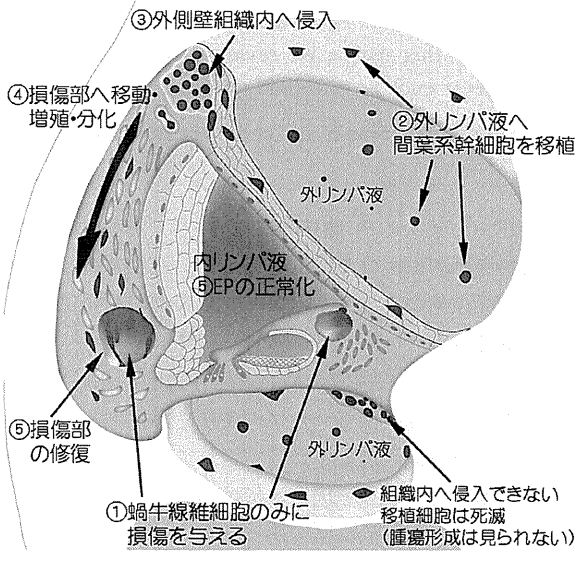

図 1　蝸牛線維細胞をターゲットとした骨髄間葉系幹細胞移植での損傷部の修復および推測された移植細胞の移動経路
薬剤投与によりらせん靭帯およびらせん板縁に選択的に損傷を与え①，その後外リンパ液へ骨髄から採取した間葉系幹細胞を半規管からの還流により投与②した結果，投与した間葉系幹細胞が外側壁組織内へ進入し④，移動・増殖・分化④により損傷部の修復⑤を促進し高周波数音域の聴力回復率が有意に上昇した．（Reprinted from Am J Pathol Am J Pathol 2007, **171**：214 ～ 226 with permission from the American Society For Investigative Pathology）

局所投与により蝸牛線維細胞の二点にのみ限局的なアポトーシスを起こすモデルラットを開発し[15)16)]，半規管からの骨髄間葉系幹細胞の外リンパ液還流投与を行った．その結果，移植 11 日後の高音域（40 KHz）の聴力回復が有意に促進し，外側壁の蝸牛線維細胞損傷部に多数の移植細胞が観察された．組織内には腫瘍化を示す移植細胞は観察されなかった．移植細胞は蝸牛外側壁の頂回転側，外リンパ液に面している部分で多くみられ，この部位を中心に蝸牛組織に侵入し損傷部まで移動したと考えられる．損傷部ではコネキシンの発現とともに隣接細胞と接合する移植細胞が観察され，イオン輸送経路の回復による内リンパ液 K^+ 濃度の正常化が聴力回復に寄与したと推測される（図 1）[3)]．

内耳への細胞投与法

著者らの初期の移植検討実験では，ラット蝸牛管付近より細胞液投与を試みた際はどの部位でも手術による永続的な聴力低下がみられ，蝸牛組織には繊維化が認められた．著者らは Iguchi らの方法[17)]を参考にラットの後半規管および外側半規管にそれぞれ小孔を開け，片側から微小チューブを挿入し細胞液（1×10^5cells/20 μl）での 10 分間の還流を行った．この方法では手術による聴力低下はほとんどみられず，大量の細胞を蝸牛内に導入することができるため内耳細胞治療に適した投与法であると思われる．また新生児難聴スクリーニング直後の早期治療を想定した内耳への投与方法として，Iizuka ら[18)]は生後 0 日齢の幼若マウスへ微小ガラス管を用いて遺伝子治療用ウイルス液を非侵襲的に外リンパ液内へ注入することに成功している．同方法は非侵襲性を必要とする幼若個体への細胞注入にも応用可能であると考えられる．この方法では外リンパ液の漏出がほとんどないため，少量であれば非侵襲的に細胞液を注入することができる．細胞移植用としてはガラス管先端の直径をパッチクランプ用のプラーで微調整することで利用可能と考えられる．

サル類を用いた細胞治療研究の重要性

げっ歯類を用いることにより，新規な細胞治療法の開発や多くの分子生物学的，生理学的データの取得が期待できる．一方でげっ歯類ではその生理・代謝機能が必ずしもヒトを忠実に反映していない部分もあり，ヒトへの外挿面で必ずしも一致した効果を得られない可能性も考えられる．たとえばヒトと同様サル類でも出生直後に外部の音刺激を入力することができると考えられるが，マウスやラットでは生後約10日齢までは内耳が未成熟であるため音の入力が開始しない．新生児難聴スクリーニング直後の細胞治療を目的とした検討の場合などはとくに成熟レベルによる細胞治療の有効性や安全性が大きく異なることが予想されるため，実験用サルによる安全性・

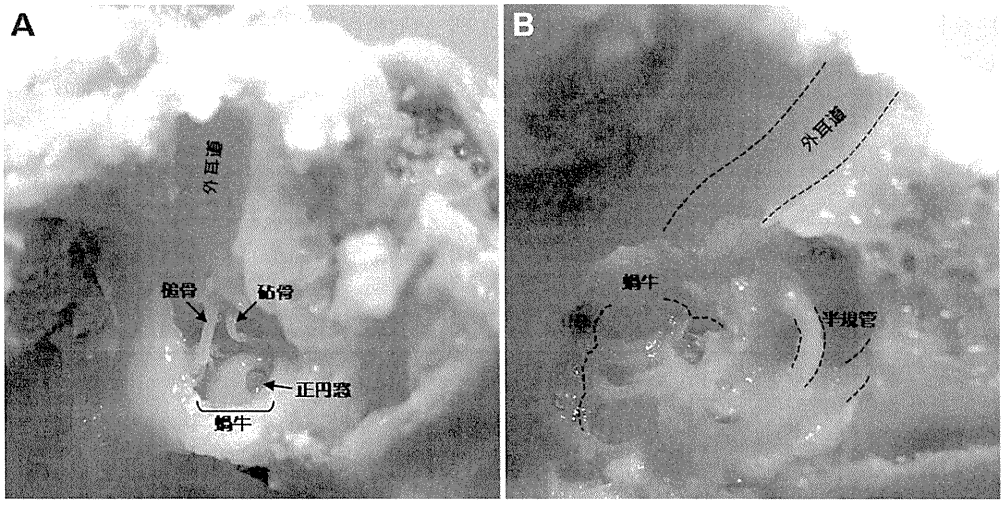

図 2　成熟カニクイザルの内耳
A．上顎側より削開し外耳道，耳小骨，蝸牛を露出した．
B．さらに内耳周囲を削開し蝸牛内部および半規管を露出した．ヒトとほぼ同様の内耳構造およびその周囲構造がみられる．

有効性の評価が将来的に非常に重要になると考えられる．マウスやラットで開発された細胞治療法を臨床応用へ近づけるためには，サル類（カニクイザル等）を用い，それらの安全性評価データをヒトへ外挿する必要がある．サル類を用いた細胞治療実験では，マウスやラットによる基礎データをもとに有効かつ安全な移植方法や移植細胞の種類，成熟ステージを評価することが重要であると考えられる．現在，カニクイザル頭部を用いた細胞治療アプローチに関する検討実験を行っている（図 2）．カニクイザル側頭骨は手術の際に削開を進める角度などがヒトと多少異なるが，内耳構造やその周囲構造に共通点が多く細胞移植手術による半規管や正円窓へのアプローチもヒトのモデルとして非常に有効であると考えられる．

各種実験動物の特徴

マウスに関していえば，近年膨大な種類の遺伝子改変マウスが各国でされ，データベース化や共有研究資材として分配されているものもある．病態変化や細胞移植後の変化を分子生物学的手法により解析する場合は情報や各種実験ツールの多さからマウスが他の実験動物と比較し圧倒的に有用性・汎用性が高いと考えられる．各種幹細胞の入手もマウスでは比較的容易である．しかし内耳への細胞の局所投与を必要とする場合はアプローチの方法やターゲットとする疾患に対し最適な病態モデルを得るため，マウス以外のげっ歯類（モルモット，スナネズミ，ラット）も十分有効に活用できる．半規管経由の細胞移植に関していえば，げっ歯類では外側半規管および後半規管が側頭骨表面に露出しているためアプローチが容易である．

サル類に関していえば，研究コスト面での負担が大きいが臨床応用へ向けての安全性・有効性評価の面で必須の実験動物といえる．カニクイザル（*Macaca fascicularis*）は我が国でも保有する施設が多数存在し，多くの動物実験に利用されている．前述したように内耳周辺の組織構造，生理機能がヒトとほぼ同等と考えられるため，げっ歯類で有効性が実証された細胞治療法をカニクイザルにおいて有効性および安全性を再評価することが臨床応用に向けて重要であると考えられる．

参考文献

1) Izumikawa M, Minoda R, Kawamoto K, et al. : Auditory hair cell replacement and hearing improvement by Atoh1 gene therapy in deaf mammals. Nat Med **11**: 271-276, 2005.
2) Gubbels SP, Woessner DW, Mitchell JC, et al. : Functional auditory hair cells produced in the mammalian cochlea by in utero gene transfer. Nature **455**: 537-541, 2008.
3) Kamiya K, Fujinami Y, Hoya N, et al. : Mesenchymal stem cell transplantation accelerates hearing recovery through the repair of injured cochlear fibrocytes. Am J Pathol **171**: 214-226, 2007.
4) Alagramam KN, Murcia CL, Kwon HY, et al. : The mouse Ames waltzer hearing-loss mutant is caused by mutation of Pcdh15, a novel protocadherin gene. Nat Genet **27**: 99-102, 2001.
5) Di Palma F, Holme RH, Bryda EC, et al. : Mutations in Cdh23, encoding a new type of cadherin, cause stereocilia disorganization in waltzer, the mouse model for Usher syndrome type 1D. Nat Genet **27**: 103-107, 2001.
6) Kikkawa Y, Shitara H, Wakana S, et al. : Mutations in a new scaffold protein Sans cause deafness in Jackson shaker mice. Hum Mol Genet **12**: 453-461, 2003.
7) Johnson KR, Gagnon LH, Webb LS, et al. : Mouse models of USH1C and DFNB18: phenotypic and molecular analyses of two new spontaneous mutations of the Ush1c gene. Hum Mol Genet **12**: 3075-3086, 2003.
8) Gibson F, Walsh J, Mburu P, et al. : A type VII myosin encoded by the mouse deafness gene shaker-1. Nature **374**: 62-64, 1995.
9) Minowa O, Ikeda K, Sugitani Y, et al. : Altered cochlear fibrocytes in a mouse model of DFN3 nonsyndromic deafness. Science **285**: 1408-1411, 1999.
10) Delprat B, Ruel J, Guitton MJ, et al. : Deafness and cochlear fibrocyte alterations in mice deficient for the inner ear protein otospiralin. Mol Cell Biol **25**: 847-853, 2005.
11) Kudo T, Kure S, Ikeda K, et al. : Transgenic expression of a dominant-negative connexin26 causes degeneration of the organ of Corti and non-syndromic deafness. Hum Mol Genet **12**: 995-1004, 2003.
12) Hequembourg S and Liberman MC : Spiral ligament pathology: a major aspect of age-related cochlear degeneration in C57BL/6 mice. J Assoc Res Otolaryngol **2**: 118-129, 2001.
13) Spicer SS and Schulte BA : Spiral ligament pathology in quiet-aged gerbils. Hear Res **172**: 172-185, 2002.
14) Wu T and Marcus DC : Age-related changes in cochlear endolymphatic potassium and potential in CD-1 and CBA/CaJ mice. J Assoc Res Otolaryngol **4**: 353-362, 2003.
15) Hoya N, Okamoto Y, Kamiya K, et al. : A novel animal model of acute cochlear mitochondrial dysfunction. Neuroreport **15**: 1597-1600, 2004.

16）Okamoto Y, Hoya N, Kamiya K, et al. : Permanent threshold shift caused by acute cochlear mitochondrial dysfunction is primarily mediated by degeneration of the lateral wall of the cochlea. Audiol Neurootol **10**: 220-233, 2005.
17）Iguchi F, Nakagawa T, Tateya I, et al. : Surgical techniques for cell transplantation into the mouse cochlea. Acta Otolaryngol Suppl 551: 43-47, 2004.
18）Iizuka T, Kanzaki S, Mochizuki H, et al. : Noninvasive in vivo delivery of transgene via adeno-associated virus into supporting cells of the neonatal mouse cochlea. Hum Gene Ther **19**: 384-390, 2008.

別刷請求先：神谷和作
〒171-0021 東京都文京区本郷2-1-1
順天堂大学医学部耳鼻咽喉科学教室

Acta Oto-Laryngologica, 2010; 130: 990–995

informa
healthcare

ORIGINAL ARTICLE

Vestibular function of patients with profound deafness related to *GJB2* mutation

MISATO KASAI[1], CHIERI HAYASHI[1], TAKASHI IIZUKA[1], AYAKO INOSHITA[1], KAZUSAKU KAMIYA[1], HIROKO OKADA[1], YUKINORI NAKAJIMA[1], KIMITAKA KAGA[2] & KATSUHISA IKEDA[1]

[1]*Department of Otorhinolaryngology, Juntendo University School of Medicine, Tokyo and* [2]*National Institute of Sensory Organs, National Tokyo Medical Center, Tokyo, Japan*

Abstract

Conclusion: GJB2 mutations are responsible not only for deafness but also for the occurrence of vestibular dysfunction. However, vestibular dysfunction tends to be unilateral and less severe in comparison with that of bilateral deafness. *Objectives:* The correlation between the cochlear and vestibular end-organs suggests that some children with congenital deafness may have vestibular impairments. On the other hand, *GJB2* gene mutations are the most common cause of nonsyndromic deafness. The vestibular function of patients with congenital deafness (CD), which is related to *GJB2* gene mutation, remains to be elucidated. The purpose of this study was to analyze the relationship between *GJB2* gene mutation and vestibular dysfunction in adults with CD. *Methods:* A total of 31 subjects, including 10 healthy volunteers and 21 patients with CD, were enrolled in the study. A hearing test and genetic analysis were performed. The vestibular evoked myogenic potentials (VEMPs) were measured and a caloric test was performed to assess the vestibular function. The percentage of vestibular dysfunction was then statistically analyzed. *Results:* The hearing level of all CD patients demonstrated a severe to profound impairment. In seven CD patients, their hearing impairment was related to *GJB2* mutation. Five of the seven patients with CD related to *GJB2* mutation demonstrated abnormalities in one or both of the two tests. The percentage of vestibular dysfunction of the patients with CD related to *GJB2* mutation was statistically higher than in patients with CD unrelated to *GJB2* mutation and in healthy controls.

Keywords: *Vestibular evoked myogenic potentials, caloric test*

Introduction

Since a correlation between the peripheral auditory and vestibular systems has been identified both anatomically and phylogenetically, a subgroup of children with congenital deafness (CD) may be associated with vestibular and balance impairments [1–3]. Interestingly, the vestibular disturbance in these children gradually disappears as they grow up, probably because of a compensatory mechanism of the central nervous system. However, there have been only a few reports that conducted a detailed analysis of the vestibular function in adults with CD.

CD has been reported in approximately one child per 1000 births [1]. In more than half of these cases, the disease is caused by gene mutation. In particular, mutation in the *GJB2* gene, which encodes Cx26 in the gap junction, is known to be a most common cause (up to 50% of such cases) [2,3]. Gap junction channels enable the neighboring cells to exchange small signaling molecules. Immunohistochemical studies have revealed that Cx26 exists not only in the cochlea but also in the vestibular organs [4]. K^+ cycling involving gap junction protein Cx26 in the vestibular labyrinth, which is similar to that in the cochlea, is thought to play a fundamental role in the endolymph homeostasis and sensory transduction [5]. These findings suggest that mutations in the *GJB2* gene may thus cause vestibular dysfunction.

Correspondence: Katsuhisa Ikeda MD PhD, 2-1-1 Hongo, Bunkyoku, Tokyo 113-8421, Japan. E-mail: ike@juntendo.ac.jp

(Received 18 October 2009; accepted 30 November 2009)

ISSN 0001-6489 print/ISSN 1651-2251 online © 2010 Informa Healthcare
DOI: 10.3109/00016481003596508

In this study, the relationship between *GJB2* gene mutation and vestibular dysfunction in adults with CD was investigated to confirm whether or not there are any abnormalities associated with the vestibular function.

Material and methods

Subjects

The subjects in this prospective study included 21 patients with CD and 10 healthy volunteers. The patients were excluded from the study if they were being treated with ototoxic drugs or if they had a cytomegalovirus infection, bacterial meningitis, external and middle ear pathological findings, or other risk factors for inner ear damage. No participants had syndromic deafness due to pigmentary retinopathy, nephropathy, goiter, or any other diseases. Patients with vestibular dysfunction due to head trauma, brain tumor, Meniere's disease, or other conditions were also excluded from the study. All subjects underwent an otoscopic examination and were found to have a normal tympanic membrane. Audiometric testing was performed in a double-walled, sound-treated booth. All patients gave their informed consent in writing and the study was approved by the Ethics Committee of Juntendo University School of Medicine.

Genetic analysis

DNA was extracted from peripheral blood leukocytes of the subjects. The coding region of *GJB2* was amplified by PCR using the primers *GJB2*-2F 5′-GTGTGCATTCGTCTTTTCCAG-3′ and *GJB2*-2R 5′-GCGACTGAGCCTTGACA-3′. The PCR products were sequenced using the PCR primers and sequence primers *GJB2*-A 5′-CCACGC-CAGCGCTCCTAGTG-3′ and *GJB2*-B 5′-GAA-GATGCTGCTGCTTGTGTAGG-3′. These were visualized using an ABI Prism 310 Analyzer (PE Applied Biosystems, Tokyo, Japan).

Vestibular evoked myogenic potentials

The vestibular evoked myogenic potentials (VEMPs) were measured as described in a previous report [6]. Both sound stimuli of clicks (0.1 ms, 95 dBnHL) and short tone burst (500 Hz; rise/fall time, 1 ms, 95 dBnHL) were presented to each side of the ear through the headphones using a Neuropack evoked-potential recorder (Nihon Kohden Co. Ltd, Tokyo, Japan). The surface electromyographic activity was recorded with the patient in the supine position from symmetrical sites over the upper half of each sternocleidomastoid (SCM) muscle with a reference electrode on the lateral end of the upper sternum. During recording, the subjects were instructed to lift their head up or to turn the contralateral side to induce hypertonicity of the SCM. Thereafter, the electromyographic signals from the stimulated side of the SCM muscle were amplified.

Caloric test

The caloric test in the current study was performed as described elsewhere [7]. Briefly, 2 ml of ice-water (at 4°C) was irrigated in the external auditory meatus to induce a thermal gradient across the horizontal semicircular canal of one ear. The duration of horizontal and vertical nystagmus was recorded. The results were compared between the right and left ears.

Statistical analysis

The data are expressed as the mean ± SD. Statistical analyses were conducted using a non-repeated measures analysis of variance (ANOVA). Significant effects were further analyzed by post hoc multiple comparison tests using the Student-Newman-Keuls test. A value of $p < 0.05$ was considered to indicate statistical significance.

Results

Hearing test

The pure-tone averages of 0.5, 1.0, and 2.0 kHz are shown in Table I. The hearing impairments of CD patients ranged from severe (71–95 dB) to profound (>95 dB). The hearing levels of all controls were at the normal level (<30 dB; data not shown).

Genetic analysis

GJB2 mutations were found in nine CD patients (Table I). All three mutations have been described previously in association with deafness. Among these mutations, 235delC mutation was found in eight patients. One nonsense mutation (Y136X) and one frameshift mutation (176-191del) were also identified. In six patients with a homozygous *GJB2* mutation and one patient with a compound heterozygous

Table I. Results of hearing level, genetic analysis, and vestibular function of subjects with congenital deafness (CD)

Case no.	Hearing level (dB) Left	Right	Sex	Age (years)	Mutation in *GJB2*	VEMPs	Caloric test
Patients with *GJB2*-related CD							
1	86	98	M	26	Homo 235delC	Right decreased	Left CP
2	106	108	M	25	Homo 235delC	Right decreased	Normal
3	108	106	M	28	Homo 235delC	Right decreased	Normal
4	108	106	M	37	Homo 235delC	Normal	Right CP
5	100	106	M	32	Homo 235delC	Normal	Right poor/left CP
6	80	91	M	25	Homo 235delC	Normal	Normal
7	115	108	M	25	Y136X/235delC	Normal	Normal
Patients without *GJB2*-related CD							
8	98	98	F	24		Left decreased	Bilateral CP
9	98	115	M	26		Normal	Bilateral CP
10	97	97	M	20		Normal	Normal
11	111	108	M	31		Normal	Normal
12	100	104	F	34		Normal	Normal
13	98	95	M	21		Normal	Normal
14	91	91	M	24		Normal	Normal
15	99	101	F	26		Normal	Normal
16	99	95	F	23		Normal	Normal
17	80	68	M	27		Normal	Normal
18	96	95	M	27		Normal	Normal
19	85	73	M	23		Normal	Normal
Patients with heterozygous *GJB2* mutation							
20	73	100	M	25	Hetero 235delC	Normal	Normal
21	97	98	M	25	Hetero 176-191del16	Normal	Normal

CP, canal paresis; Poor, nystagmus was obviously weak.

mutation (case nos 1–7); their profound deafness was thought to be caused by a *GJB2* mutation. No *GJB2* mutation was identified in any of the controls.

Vestibular function

No patients or controls had any subjective symptoms of vertigo. Table I shows the results of the vestibular function in all CD patients. Abnormal responses of VEMPs and the caloric test in CD with a *GJB2*-related mutation were observed in three patients each (case nos 1–5). Three patients with a homozygous *GJB2* mutation showed asymmetrical responses in VEMPs (case nos 1–3). Three patients with a homozygous *GJB2* mutation showed asymmetrical responses in the caloric test (case nos 1, 4, and 5). One of them showed both VEMPs and the caloric test asymmetrical responses (case no. 1). One patient with a homozygous *GJB2* mutation and one patient with compound heterozygous *GJB2* mutation showed normal responses in both VEMPs and the caloric test (case nos 6 and 7). It is notable that five of the six patients with a homozygous 235delC mutation showed no abnormalities in either test. Two heterozygous patients (case nos 20 and 21) showed normal responses in both tests.

Two CD patients with no *GJB2* mutation exhibited abnormal findings for the vestibular tests (case nos. 8 and 9). One patient showed a unilateral reduction in VEMPs and bilateral canal paresis (case no. 8). Bilateral canal paresis was also observed in another patient (case no. 9).

All the controls with normal hearing showed normal responses in both the VEMPs and the caloric test (data not shown).

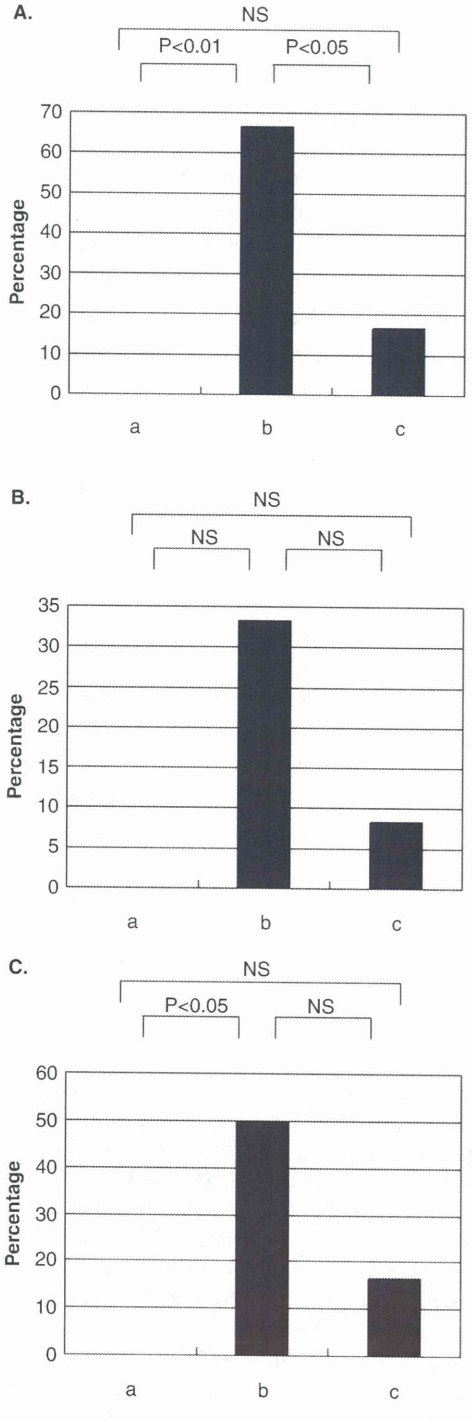

Figure 1. Comparison of the incidence of abnormality in the vestibular tests among the three groups. (A) Percentage showing abnormality in VEMPS and/or caloric test. (B) Percentage showing abnormality in VEMPs. (C) Percentage showing abnormality in the caloric test. a, Controls; b, *GJB2*-related CD subjects; c, CD subjects without *GJB2* mutations.

Statistical analysis of vestibular function in the three groups

Figure 1 shows a comparison of the controls, patients with CD related to a *GJB2* mutation, and those with CD without a *GJB2* mutation. The CD patients with *GJB2* heterozygous mutation were excluded from this statistical analysis, since their symptoms of hearing impairment are not necessarily caused by the *GJB2* mutation alone. Vestibular dysfunction showing an abnormality in VEMP and/or the caloric test significantly increased in patients with *GJB2*-related CD in comparison with those with CD without *GJB2* mutation ($p < 0.05$) and the controls ($p < 0.01$), whereas no difference was observed between CD without a *GJB2* mutation and the controls (Figure 1A). No differences in the incidence of abnormality in VEMPs were observed among the three groups (Figure 1B). The incidence of abnormalities in the caloric test in patients with *GJB2*-related CD differed significantly from that in the controls, but the other two comparisons were not significant (Figure 1C).

Discussion

In this study, vestibular tests were performed in CD patients with or without a *GJB2* mutation by measuring the VEMPs and using the caloric test. Only one report has previously investigated the vestibular function of patients with *GJB2*-related CD [8]. The authors noted that five of the seven patients showed no VEMP responses bilaterally and that only one case had a unilateral pathological response in the caloric test, which led to the conclusion that CD with a *GJB2* mutation is associated with severe saccular dysfunction. However, in the present study, there were no patients showing the absence of both VEMP and a caloric response. Todt et al. [8] showed the existence of *GJB2* mutations that do not cause CD (polymorphisms), thus suggesting a considerable bias. Furthermore, patients with low-grade hearing loss were included in their study. In contrast, all of the *GJB2* mutations detected in the present study are known to cause CD in the Asian population [9]. In addition, the present study included only patients with severe to profound hearing loss, which would therefore clarify the correlation between CD and *GJB2* mutations. Among the seven patients with *GJB2*-related CD, five (71.4%) showed abnormal responses in either or both tests. The incidence was apparently and significantly higher than that in patients with CD without a *GJB2* mutation (2/13: 15.4%). Moreover, the incidence in the controls significantly differed from that in patients with CD related to a *GJB2*

mutation but not in those with CD without *GJB2* mutation. Therefore, these findings support the hypothesis that *GJB2* mutations play a critical role in the disturbance of the vestibular function.

GJB2 mutations cause profound deafness and the associated mechanism has been discussed in several studies [10,11]. A recent study showed that *GJB2* is indispensable in the normal development of the organ of Corti and normal hearing on the basis of the study in *Gjb2* dominant-negative mutant mice [12]. Despite the widespread expression of Cx26 in both the cochlear and vestibular organs [4], the vestibular function impairment of the patients with a *GJB2* mutation is not as severe as the hearing dysfunction observed in the present study. Two hypotheses have been proposed to explain this inconsistency between hearing and balance function. One hypothesis is based on the fact that two temporal bone studies performed in patients with *GJB2*-related hearing impairment in the previous study revealed that one patient had mild vestibular hydrops and saccular degeneration, while another patient had a dysplastic neuroepithelium of the saccule [13,14]. This suggests that a *GJB2* mutation can cause morphological dysplasia in not an entire organ, but in part of the vestibular organs. This is contrast to the cochlea of these patients, which showed nearly total dysplasia of the organ of Corti. These histopathological studies support the results of the vestibular dysfunction of patients with *GJB2*-related CD in the present study. The other hypothesis is based on the presence of several connexins such as Cx26, Cx30 (encoded by *GJB6*), Cx31 (encoded by *GJB3*), and Cx32 (encoded by *GJB1*) in the inner ear. A previous study showed all of these connexins to be distributed in the vestibular organs [15]. Cx30 gene knockout mice had hair cell loss in the saccule, which was restored by the over-expression of the Cx26 gene [16]. Therefore, the specific loss of Cx30 causes vestibular dysfunction, which can be compensated by other types of connexins. The present clinical study in which a complete defect of Cx26 resulted in a definitive but partial dysfunction of vestibular end organs can be explained by the compensation of other connexins normally expressed in the vestibule. Further studies are required to clarify the relationship between connexins and the vestibular function.

Although there was a statistically significant difference in the objective examination of the vestibular function among patients with *GJB2*-related CD, those with CD without a *GJB2* mutation, and healthy controls, none of these subjects had any vestibular symptoms regardless of the presence or absence of a *GJB2* mutation. The peripheral vestibular dysfunction predicted in individuals with the *GJB2* mutation may be compensated by the central vestibular system in young patients with deafness, as shown in the present study. However, aging is known to affect both the peripheral and central vestibular system [17]. In patients with a *GJB2* mutation, the vestibular symptoms may progress with aging. Another problematic point regarding patients with CD related to *GJB2* mutations is cochlear implantation, which has been reported to cause vestibular dysfunction, such as a reduction of the caloric responses [18] and a decrease in the VEMP responses [19]. It is thought that the mechanical damage caused by the insertion of the electrode may induce vestibular dysfunction [20]. In the present study, four patients with *GJB2*-related deafness showed unilateral vestibular dysfunction, while only one of them had bilateral dysfunction. Therefore, it should be emphasized that the assessment of the vestibular function in patients with *GJB2*-related CD is important to determine which side of the ear should be selected to insert the cochlear implant.

Conclusions

A *GJB2* mutation is responsible not only for deafness but also for vestibular dysfunction. However, such vestibular dysfunction is likely to be unilateral and less severe in patients with a *GJB2* mutation than in those with bilateral deafness.

Declaration of interest: The authors report no conflicts of interest. The authors alone are responsible for the content and writing of the paper.

References

[1] Morton NE. Genetic epidemiology of hearing impairment. Ann N Y Acad Sci 1991;630:16–31.

[2] Denoyelle F, Marlin S, Weil D, Moatti L, Chauvin P, Garabedian EN, et al. Clinical features of the prevalent form of childhood deafness, DFNB1, due to a connexin-26 gene defect: implications for genetic counselling. Lancet 1999;353:1298–303.

[3] Murgia A, Orzan E, Polli R, Martella M, Vinanzi C, Leonardi E, et al. Cx26 deafness: mutation analysis and clinical variability. J Med Genet 1999;36:829–32.

[4] Masuda M, Usami S, Yamazaki K, Takumi Y, Shinkawa H, Kurashima K, et al. Connexin 26 distribution in gap junctions between melanocytes in the human vestibular dark cell area. Anat Rec 2001;262:137–46.

[5] Wangemann P. K(+) cycling and its regulation in the cochlea and the vestibular labyrinth. Audiol Neurootol 2002;7:199–205.

[6] Jin Y, Nakamura M, Shinjo Y, Kaga K. Vestibular-evoked myogenic potentials in cochlear implant children. Acta Otolaryngol 2006;126:164–9.

[7] Yukiko S, Yulian J, Kimitaka K. Assessment of vestibular function of infants and children with congenital and acquired deafness using the ice-water caloric test, rotational chair test and vestibular-evoked myogenic potential recording. Acta Otolaryngol 2007;127:736–47.

[8] Todt I, Hennies HC, Basta D, Ernst A. Vestibular dysfunction of patients with mutations of Connexin 26. Neuroreport 2005;16:1179–81.

[9] Ohtsuka A, Yuge I, Kimura S, Namba A, Abe S, Van Later L, V, et al. GJB2 deafness gene shows a specific spectrum of mutations in Japan, including a frequent founder mutation. Hum Genet 2003;112:329–33.

[10] Kudo T, Kure S, Ikeda K, Xia AP, Katori Y, Suzuki M, et al. Transgenic expression of a dominant-negative connexin26 causes degeneration of the organ of Corti and non-syndromic deafness. Hum Mol Genet 2003;12:995–1004.

[11] Cohen-Salmon M, Ott T, Michel V, Hardelin JP, Perfettini I, Eybalin M, et al. Targeted ablation of connexin26 in the inner ear epithelial gap junction network causes hearing impairment and cell death. Curr Biol 2002;12: 1106–11.

[12] Inoshita A, Iizuka T, Okamura HO, Minekawa A, Kojima K, Furukawa M, et al. Postnatal development of the organ of Corti in dominant-negative Gjb2 transgenic mice. Neuroscience 2008;156:1039–47.

[13] Griffith AJ, Yang Y, Pryor SP, Park HJ, Jabs EW, Nadol JB Jr, et al. Cochleosaccular dysplasia associated with a connexin 26 mutation in keratitis-ichthyosis-deafness syndrome. Laryngoscope 2006;116:1404–8.

[14] Jun AI, McGuirt WT, Hinojosa R, Green GE, Fischel-Ghodsian N, Smith RJ. Temporal bone histopathology in connexin 26-related hearing loss. Laryngoscope 2000;110:269–75.

[15] Forge A, Becker D, Casalotti S, Edwards J, Marziano N, Nevill G. Gap junctions in the inner ear: comparison of distribution patterns in different vertebrates and assessment of connexin composition in mammals. J Comp Neurol 2003;467:207–31.

[16] Qu Y, Tang W, Dahlke I, Ding D, Salvi R, Sohl G, et al. Analysis of connexin subunits required for the survival of vestibular hair cells. J Comp Neurol 2007;504: 499–507.

[17] Gazzola JM, Perracini MR, Gananca MM, Gananca FF. Functional balance associated factors in the elderly with chronic vestibular disorder. Braz J Otorhinolaryngol 2006;72:683–90.

[18] Buchman CA, Joy J, Hodges A, Telischi FF, Balkany TJ. Vestibular effects of cochlear implantation. Laryngoscope 2004;114:1–22.

[19] Ernst A, Todt I, Seidl RO, Eisenschenk A, Blodow A, Basta D. The application of vestibular-evoked myogenic potentials in otoneurosurgery. Otolaryngol Head Neck Surg 2006;135:286–90.

[20] Jin Y, Shinjo Y, Akamatsu Y, Ogata E, Nakamura M, Kianoush S, et al. Vestibular evoked myogenic potentials evoked by multichannel cochlear implant – influence of C levels. Acta Otolaryngol 2008;128:284–90.

Biochemical and Biophysical Research Communications 389 (2009) 569–574

Contents lists available at ScienceDirect

Biochemical and Biophysical Research Communications

journal homepage: www.elsevier.com/locate/ybbrc

Mutation-induced reinforcement of prestin-expressing cells

Shun Kumano [a], Xiaodong Tan [b], David Z.Z. He [b], Koji Iida [a], Michio Murakoshi [a], Hiroshi Wada [a,*]

[a] Department of Bioengineering and Robotics, Tohoku University, Sendai, Japan
[b] Department of Biomedical Sciences, Creighton University, Omaha, NE, USA

ARTICLE INFO

Article history:
Received 30 August 2009
Available online 6 September 2009

Keywords:
Inner ear
Outer hair cell
Prestin
Electrophysiological property
Somatic motility
Point mutation

ABSTRACT

The motor protein prestin in cochlear outer hair cells is a member of the solute carrier 26 family, but among the proteins of that family, only prestin can confer the cells with nonlinear capacitance (NLC) and motility. In the present study, to clarify contributions of unique amino acids of prestin, namely, Met-122, Met-225 and Thr-428, to the characteristics of prestin, mutations were introduced into those amino acids. As a result, NLC remained unchanged by both replacement of Met-122 by isoleucine and that of Thr-428 by leucine, suggesting that those amino acids were not important for the generation of NLC. Surprisingly, the replacement of Met-225 by glutamine statistically increased NLC as well as the motility of prestin-expressing cells without an increase in the amount of prestin expression in the plasma membrane. This indicates that Met-225 in prestin somehow adjusts NLC and the motility of prestin-expressing cells.

Introduction

Prestin is the motor protein expressed in the plasma membrane of outer hair cells (OHCs) [1]. A voltage-dependent conformational change of prestin in the plasma membrane is believed to induce OHC electromotility, which is known to be a key element of cochlear amplification [2]. OHCs as well as culture cells engineered to express prestin show electromotility [3], supporting the idea that prestin is the origin of such motility. Although prestin is regarded as one of 11 members of the solute carrier 26 (SLC26) family [4], prestin is the only member of that family which can confer the cells with motility. Nonlinear capacitance (NLC) observed in prestin-expressing cells, which is highly associated with their motility, is often measured for the analysis of prestin activity [5]. To date, several studies on prestin have been performed for its characterization. Mutational studies on prestin have indicated the importance of its N-terminal and C-terminal cytoplasmic domain, identified its glycosylation sites and phosphorylation sites, etc. [6–11], and electron microscopy and atomic force microscopy have revealed the shape of prestin [12,13]. Despite such studies, how prestin confers the cells with motility and NLC has remained unknown.

As conferring cells with motility and NLC is the specific function of prestin in the SLC26 family, unique amino acids in prestin are considered to realize such function. In the present study, to clarify the contributions of such unique amino acids to the characteristics of prestin, point mutations were introduced into those amino acids which were selected by the comparison of the amino acid sequences among the SLC26 proteins. The characteristics of the prestin mutants were then compared with those of wild-type prestin (WT).

Materials and methods

Multiple alignment of the amino acid sequence of the SLC26 family proteins. To select amino acids which are unique in prestin among the SLC26 family, multiple alignment using genes of 11 members of that family was performed by use of the ClustalX Multiple Sequence Alignment Program [14]. In the result of the alignment, the transmembrane domains of prestin in its predicted membrane topology [11] were focused on, as N- and C-terminal cytoplasmic domains have already been well investigated [6–8]. In those domains, the amino acids of prestin were compared with those at corresponding positions of the other SLC26 proteins. By such comparison, we attempted to identify the positions of amino acids where the majority of the SLC26 proteins have the same amino acids but prestin has different amino acids. Such amino acids in prestin were considered to be unique.

Abbreviations: NLC, nonlinear capacitance; OHCs, outer hair cells; SLC26, solute carrier 26; WT, wild-type prestin; FBS, fetal bovine serum; WGA, wheat germ agglutinin; DBcGMP, N^2,2′-*O*-dibutyrylguansine 3′,5′-cyclic monophosphate sodium salt hydrate.

* Corresponding author. Address: Department of Bioengineering and Robotics, Tohoku University, 6-6-01 Aoba-yama, Sendai 980-8579, Japan. Fax: +81 22 795 6939.

E-mail addresses: kumano@wadalab.mech.tohoku.ac.jp (S. Kumano), xiaodong Tan@creighton.edu (X. Tan), davidhe@creighton.edu (D.Z.Z. He), iida@wadalab.mech.tohoku.ac.jp (K. Iida), michio@wadalab.mech.tohoku.ac.jp (M. Murakoshi), wada@cc.mech.tohoku.ac.jp (H. Wada).

0006-291X/$ - see front matter © 2009 Elsevier Inc. All rights reserved.
doi:10.1016/j.bbrc.2009.09.016

Construction of prestin mutant genes. Three genes of prestin mutants, namely, genes of M122I, M225Q and T428L, were constructed by overlap PCR. Constructed prestin mutant genes were ligated into mammalian expression vector pIRES-hrGFP-1a (Stratagene, La Jolla, CA). In addition, to detect prestin by antibodies in immunofluorescence staining and Western blotting, genes expressing the prestin mutants, the C-terminus of which was fused to FLAG-tag, were generated. Such genes were also ligated into the expression vector. The sequences of the constructed genes were confirmed by an automated DNA sequencer (Applied Biosystems, Foster City, CA).

Cell culture and transfection. HEK293 cells were cultured in RPMI-1640 medium (Sigma–Aldrich, St. Louis, MO) supplemented with culture medium consisting of 10% fetal bovine serum (FBS), 100 U/ml penicillin and 100 μg/ml streptomycin at 37 °C with 5% CO_2. One hour before transfection, the culture medium was changed to RPMI-1640 medium supplemented only with 10% FBS. The expression vectors were transfected into HEK293 cells using Fugene HD Transfection Reagent (Roche, Indianapolis, IN) according to the manufacturer's instructions.

Measurement of nonlinear capacitance. NLC in prestin-transfected HEK293 cells, which is commonly used for the evaluation of the function of prestin, was measured by the whole-cell patch-clamp method 36–48 h after transfection, as described previously [15]. The membrane capacitance recorded from the transfected cells was fitted with the first derivative of the Boltzmann function [5],

$$C_m(V) = C_{lin} + \frac{Q_{max}}{\alpha e^{\frac{V-V_{1/2}}{\alpha}}\left(1+e^{\frac{V-V_{1/2}}{\alpha}}\right)^2}, \quad (1)$$

where C_{lin} is the linear capacitance, which is proportional to the membrane area of the cells, Q_{max} is the maximum charge transfer, V is the membrane potential and $V_{1/2}$ is the voltage at half-maximal charge transfer. In Eq. (1), α is the slope factor of the voltage-dependent charge transfer and is given by

$$\alpha = kT/ze, \quad (2)$$

where k is Boltzmann constant, T is absolute temperature, z is valence and e is electron charge. When the NLC curves of the prestin mutants were compared with that of WT, the normalized NLC $C_{nonlin/lin}$ was defined as

$$C_{nonlin/lin}(V) = \frac{C_{nonlin}}{C_{lin}} = \frac{(C_m(V) - C_{lin})}{C_{lin}}, \quad (3)$$

where C_{nonlin} is the nonlinear component of the measured membrane capacitance. In addition, $C_{nonlin/lin}(V)$ was divided by the maximum $C_{nonlin/lin}(V)$ of WT and termed relative $C_{nonlin/lin}(V)$. To evaluate the maximum charge transfer of prestin in the unit plasma membrane, Q_{max}, which is the maximum charge transfer of prestin in whole plasma membrane, was normalized by C_{lin} and designated as charge density.

Motility measurement. Electromotility of the prestin mutant-expressing cells was compared with that of WT-expressing cells using a microchamber configuration 36–48 h after transfection. The motility measurement in such configuration was performed as described previously [16]. In the present study, the electrical stimulus was a 100-Hz sinusoidal voltage burst of 100 ms duration. Voltage commands of ±400 mV were used. Since approximately 50% of the cells were inserted into the microchamber, the resultant voltage drops on the extruded segment were estimated to be 50% of the voltage applied, or ±200 mV [17].

Western blotting. The amount of WT and that of its mutant in transfected cells were evaluated by Western blotting. Forty-eight hours after transfection, 5×10^4 cells were dissolved in SDS sample buffer and used for SDS–PAGE and Western blotting. A prestin band was detected by anti-FLAG mouse monoclonal antibody (Sigma–Aldrich) and HRP-conjugated anti-mouse IgG antibody (Cell Signaling Technology, Beverly, MA). In addition, a β-actin band was detected by anti-β-actin antibody (Sigma–Aldrich) and HRP-conjugated anti-mouse IgG antibody. Those bands were visualized by enhanced chemiluminescence using an ECL Western blotting detection kit (GE Healthcare Bio-Science AB). Western blotting images were obtained with a luminescent image analyzer (Chem-iDoc XRS, Bio-Rad Laboratories, Hercules, CA) and the band intensity was then analyzed. To eliminate the effects of the difference in the concentration of proteins between samples on the comparison of the band intensity, the intensity of the bands in WT and M225Q was normalized by that of β-actin, which is generally used as a control protein. Afterwards, relative intensity was obtained by dividing the normalized intensity of the WT band and that of the M225Q band by the average of the normalized intensity of the WT band.

Immunofluorescence experiment. The localization of WT and that of its mutant in transfected cells were investigated by immunofluorescence staining 48 h after transfection. Plasma membranes of the cells were stained with wheat germ agglutinin (WGA)-Alexa Fluor 633 conjugate (Invitorogene), which has been used for a plasma membrane marker as well as a Golgi body marker. After fixation of the cells with 4% paraformaldehyde and blocking by a buffer consisting of 50% Block Ace (Dainippon Pharmaceutical, Osaka, Japan) and 50% fetal bovine serum, prestin was stained by anti-FLAG antibody (Sigma–Aldrich) in PBS with 0.1% saponin solution and TRITC-conjugated anti-mouse IgG antibody (Sigma–Aldrich) in PBS with 0.1% saponin solution. The stained cells were

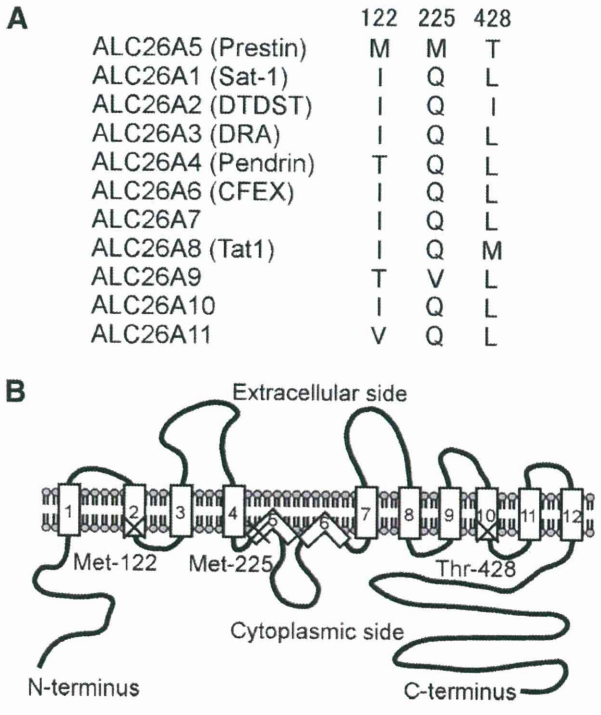

Fig. 1. Comparison of the amino acid sequences of the SLC26 proteins and the positions of the amino acids in prestin focused on in the present study. (A) Multiple alignment of the amino acid sequence of SLC26 proteins. Amino acid residue numbers refer to amino acids of prestin. Methionine was found at positions of 122 and 225 in prestin, while isoleucine and glutamine were detected at the corresponding positions of most of the other SLC26 proteins, respectively. In addition, prestin has threonine at position of 428, but most of the other SLC26 proteins have leucine at the corresponding positions. (B) Predicted membrane topology of prestin [11]. The positions of Met-122, Met-225 and Thr-428 in prestin are shown by "X" in its predicted membrane topology.

then observed using a confocal laser scanning microscope (FV500, Olympus, Tokyo, Japan). Detected TRITC fluorescence and Alexa Fluor 633 fluorescence were indicated by red and green, respectively.

In the present study, the ratio of the amount of prestin localized in the plasma membrane to the total amount of prestin in the cell, R_p, was investigated. The R_p was calculated by the following equation:

$$R_p = \frac{I_p}{I_w}, \tag{4}$$

where I_w is the summation of the intensity of TRITC fluorescence of the whole area of the target cell which reflects the total amount of prestin in the cell, and I_p is the summation of the intensity of TRITC fluorescence of only pixels corresponding to the plasma membrane, which reflects the amount of prestin there. For the calculation of I_w and I_p, the average intensity value of the background noise of TRITC fluorescence was first subtracted from the intensity value of TRITC fluorescence in all pixels in the obtained images. In the subtracted images, only pixels whose intensity values of TRITC fluorescence were 6 times greater than such background noise were used for the calculation of I_w and I_p. I_w was obtained by summing up the intensity values of TRITC fluorescence of the whole areas of the target cells in the subtracted images. To calculate I_p, the pixels which corresponded to the plasma membrane had to be defined. The plasma membrane and the Golgi body of the cells were stained by WGA-Alexa Fluor 633 conjugate in this experiment. As the plasma membrane and the Golgi body are at different positions in the cells, the positions of the pixels corresponding to the plasma membrane were identifiable. I_p was obtained by summing up the intensity values of TRITC fluorescence of the pixels corresponding to the plasma membrane which had an intensity value of Alexa Fluor 633 fluorescence 2 times greater than its background noise.

Results and discussion

As a result of the multiple alignments of the amino acid sequences of the SLC26 family proteins, we found that methionine was present at positions of 122 and 225 of prestin, but that the majority of the other SLC26 proteins had isoleucine and glutamine at the corresponding positions, respectively (Fig. 1). In addition, prestin has threonine at position of 428, but leucine was found at the corresponding positions in the majority of the other SLC26 proteins. The side chains of amino acids in prestin described above have different characteristics from those of the corresponding amino acids in the other SLC26 proteins. Thus, Met-122, Met-225 and Thr-428 of prestin were considered to be unique in the SLC26 family, therefore implying that they are responsible for the unique functions of prestin. In the present study, to clarify roles of Met-122, Met-225 and Thr-428 in prestin, mutations were introduced into those amino acids, resulting in three prestin mutants, namely, M122I, M225Q and T428L. Characteristics of those prestin mutants were then investigated.

Fig. 2 shows recorded NLC curves and the fitting parameters obtained in WT-expressing cells and prestin mutant-expressing cells. In addition to WT, all mutants prepared in the present study showed NLC (Fig. 2A). Compared with the $V_{1/2}$ of WT, that of M122I and M225Q and that of T428L were statistically shifted in the hyperpolarization and depolarization direction, respectively ($p < 0.05$) (Fig. 2B). In addition, T428L showed a statistically smaller α than that of WT ($p < 0.05$) (Fig. 2C). The changes in the $V_{1/2}$ and α indicate changes in the reactivity of prestin to the membrane

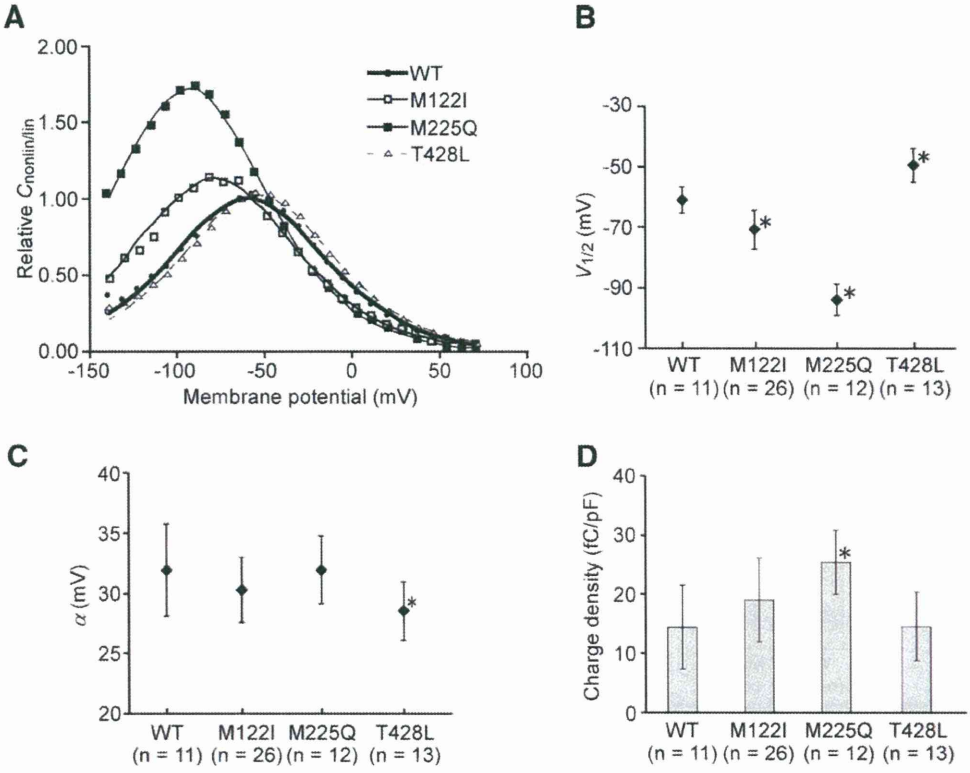

Fig. 2. Results of the whole-cell patch-clamp recording. (A) NLC curves. Not only WT but also all prestin mutants showed NLC. (B) $V_{1/2}$. M122I and M225Q and T428L showed $V_{1/2}$ statistically shifted in the hyperpolarization and depolarization direction, respectively ($p < 0.05$). (C) α. The α of T428L was statistically smaller than that of WT ($p < 0.05$). (D) Charge density. Interestingly, M225Q showed statistically larger charge density than that of WT ($p < 0.05$). In contrast, there was no statistical difference between WT and the other mutants.

potential and anions. As methionine and threonine do not have charge, the mutations of Met-122, Met-225 and Thr-428 might affect the structure of prestin, but not as greatly as the abolishment of NLC, and thus alter such reactivity. As shown in Fig. 2D, the charge density of M122I and T428L was similar to that of WT, suggesting that Met-122 and Thr-428 are not required for the generation of NLC. On the other hand, interestingly, the charge density of M225Q was significantly larger than that of WT ($p < 0.05$). To confirm if the motility of prestin-expressing cells was also increased by the mutation in Met-225, that motility was measured in the microchamber configuration. Results showed that the displacement of M225Q-expressing cells due to the variation in the membrane potential was statistically greater than that of WT-expressing cells ($p < 0.05$) (Fig. 3), suggesting that the replacement of Met-225 by glutamine significantly enhanced the charge density and the motility of prestin-expressing cells. This result implies that one reason why prestin has methionine instead of glutamine at position 225 may be to somehow adjust the charge density and the motility of prestin-expressing cells.

To understand the contributions of Met-225 to prestin in more detail, the mechanism of the increase in the charge density and the motility of prestin-expressing cells by the mutation in Met-225 were investigated. First, the amount of M225Q and WT in the cells was analyzed by comparing the band intensity of M225Q with that of WT in Western blotting (Fig. 4A and B). No statistical difference in the band intensity was detected between WT and M225Q, suggesting that the amount of M225Q in the cells was similar to that of WT. In addition, the localization of M225Q in the cells was compared with that of WT by immunofluorescence staining. Fig. 4C and D shows representative images of stained cells and R_p, which is the ratio of the amount of prestin in the plasma membrane to the total amount of prestin in the cells. The R_p of M225Q was similar to that of WT, meaning that the localization pattern was unchanged by the mutation in Met-225. Thus, the replacement of Met-225 by glutamine was found not to change the amount of prestin and its localization pattern in the cells.

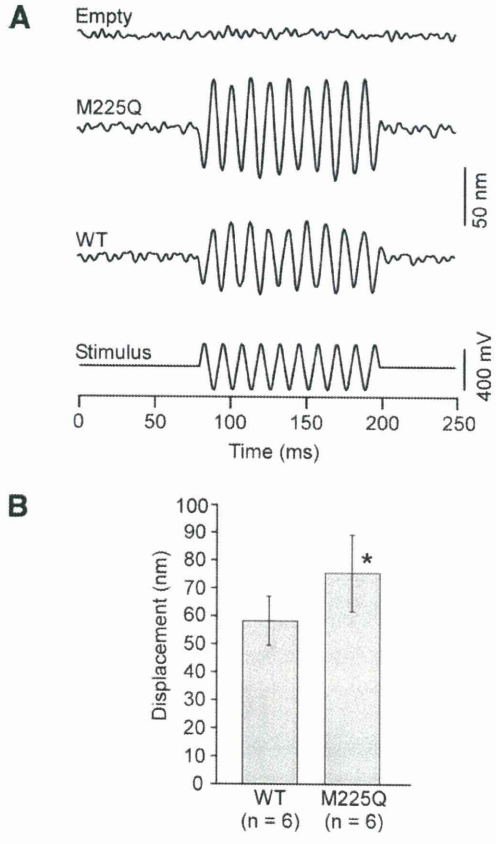

Fig. 3. Motile response of WT-expressing cells and M225Q-expressing cells. (A) Results of measurement of the motility of prestin-expressing cells. Unlike empty vector-transfected cells, WT-expressing cells and M225Q-expressing cells exhibited motile response to changes in their membrane potential. (B) Comparison of the displacement of WT-expressing cells and M225Q-expressing cells. The displacement of M225Q-expressing cells was statistically larger than that of WT-expressing cells ($p < 0.05$).

In the present study, we found that the charge density and the motility of prestin-expressing cells statistically increased by the mutation in Met-225, but that the amount of prestin and its localization pattern in the cells remained unchanged. This means that such increase cannot be explained by the increase of the amount of prestin in the plasma membrane. Due to uniqueness of our results, they might be considered to be implausible. However, the observed interesting phenomena, namely, the increase in the charge density of prestin-expressing cells without an increase of prestin in the plasma membrane, has been found so far in conditions different from those of the present study. Oliver et al. [18] showed that in the inside-out patch-clamp recording for OHCs, Q_{max} increased by changing anions from Cl^- to I^- in the solution on the cytoplasmic surface of the membrane. The increase of Q_{max} in the inside-out patch-clamp recording has the same meaning as the increase of the charge density because in such recording, C_{lin} is almost constant between the samples and the charge density is calculated by the division of Q_{max} by C_{lin}. In inside-out patch-clamp recording, it is unlikely that the amount of prestin in the plasma membrane increases during such recording. That is, in the study of Oliver et al., the charge density increased without an increase in the amount of prestin in the plasma membrane. Moreover, Deák et al. [11] showed that the charge density increased when N^2,2′-*O*-dibutyrylguansine 3′,5′-cyclic monophosphate sodium salt hydrate (DBcGMP), which induces the phosphorylation of prestin, was contained in the patch pipette in the whole-cell patch-clamp recording. Such increase was recordable from 5 s after establishment of the whole-cell patch-clamp configuration, ruling out the possibility that the increase of the charge density resulted from the increase in the amount of prestin in the plasma membrane caused by DBcGMP because 5 s was insufficient for the translocation of proteins caused by cGMP [19]. Thus, those two studies showed that it was possible that the charge density increased by some manipulations without the increase in the amount of prestin in the plasma membrane, enhancing the credibility of our interesting results. To interpret our study and two studies mentioned above, it should be considered that both functional and non-functional prestin exist in the plasma membrane. If the ratio of the amount of functional prestin to the total amount of functional and non-functional prestin in the plasma membrane increases, the charge density and the motility of prestin-expressing cells can increase without an increase in the total amount of these two types of prestin. The study of Oliver et al. may indicate that as the amount of prestin interacting with I^- is larger than that of prestin interacting with Cl^- in the plasma membrane, changing anions from Cl^- to I^- led to the increase in the amount of prestin interacting with anions, namely, the increase of the amount of functional prestin in the plasma membrane. The study of Deák et al. may mean that the phosphorylation of prestin somehow increased the ratio of the amount of functional prestin to the total amount of functional and non-functional prestin in the plasma membrane. Also in the present study, the replacement of Met-225 by glutamine was speculated to increase such ratio, resulting in the increase in the charge density as well as in the motility of prestin-expressing cells, which implies that Met-225 adjusts the charge density and the motility, probably by controlling such ratio.

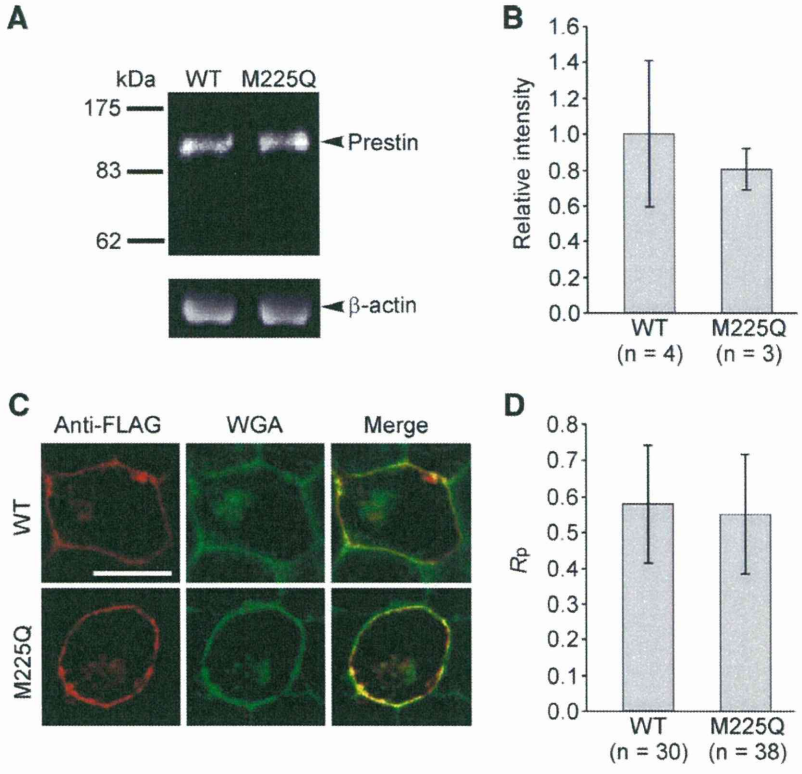

Fig. 4. Amount of prestin and its localization in the cells. (A) Western blotting using whole-cell lysate of prestin-expressing cells. The 100 kDa bands were found in both WT and M225Q. (B) Comparison of the intensity of bands. The intensity of bands of WT and M225Q was normalized by that of β-actin bands, and then relative intensity was obtained by dividing the normalized intensity of the WT band and that of the M225Q band by the average of the normalized intensity of the WT band. There was no statistical difference in the relative intensity between WT and M225Q. (C) Representative images of a stained WT-expressing cell and a M225Q-expressing cell. Red fluorescence indicates prestin and green indicates the plasma membrane and the Golgi body. In merged images, orange-yellow fluorescence shows the co-localization of prestin and the plasma membrane and that of prestin and the Golgi body, scale bar shows 10 μm. (D) Ratio of the amount of prestin localized in the plasma membrane to the total amount of prestin in the cell, R_p. The R_p of M225Q was similar to that of WT, indicating that the localization pattern was unchanged by the mutation.

In summary, we introduced point mutations into the unique amino acids in prestin, Met-122, Met-225 and Thr-428. As a result, the replacement of Met-225 in prestin by glutamine was found to remarkably increase the charge density and the motility of prestin-expressing cells without an increase of prestin in the plasma membrane, implying that Met-225 in prestin somehow adjusts the charge density and the motility. In addition, our results showed that Met-122 and Thr-428 are not required for prestin to confer cells with NLC.

Acknowledgments

This work was supported by Grant-in-Aid for Scientific Research (B) 18390455 from the Japan Society for the Promotion of Science, by Grant-in-Aid for Exploratory Research 18659495 from the Ministry of Education, Culture, Sports, Science and Technology of Japan, by a grant from the Human Frontier Science Program, by a Health and Labour Science Research Grant from the Ministry of Health, Labour and Welfare of Japan and by Tohoku University Global COE Program "Global Nano-Biomedical Engineering Education and Research Network Centre" to H.W., and by a Grant-in-Aid for JSPS Fellows from the Japan Society for the Promotion of Science to S.K.

References

[1] J. Zheng, W. Shen, D.Z.Z. He, K.B. Long, L.D. Madison, P. Dallos, Prestin is the motor protein of cochlear outer hair cells, Nature 405 (2000) 149–155.
[2] P. Dallos, B. Fakler, Prestin, a new type of motor protein, Nat. Rev. Mol. Cell Biol. 3 (2002) 104–111.
[3] J. Ludwig, D. Oliver, G. Frank, N. Klöcker, A.W. Gummer, B. Fakler, Reciprocal electromechanical properties of rat prestin: the motor molecule from rat outer hair cells, Proc. Natl. Acad. Sci. USA 98 (2001) 4178–4183.
[4] D.B. Mount, M.F. Romero, The SLC26 gene family of multifunctional anion exchangers, Pflugers Arch. 447 (2004) 710–721.
[5] J. Santos Sacchi, Reversible inhibition of voltage-dependent outer hair cell motility and capacitance, J. Neurosci. 11 (1991) 3096–3110.
[6] J. Zheng, G.G. Du, K. Matsuda, A. Orem, S. Aguiñaga, L. Deák, E. Navarrete, L.D. Madison, P. Dallos, The C-terminus of prestin influences nonlinear capacitance and plasma membrane targeting, J. Cell Sci. 118 (2005) 2987–2996.
[7] D. Navaratnam, J.P. Bai, H. Samaranayake, J. Santos Sacchi, N-terminal-mediated homomultimerization of prestin, the outer hair cell motor protein, Biophys. J. 89 (2005) 3345–3352.
[8] J.P. Bai, D. Navaratnam, H. Samaranayake, J. Santos Sacchi, En block C-terminal charge cluster reversals in prestin (SLC26A5): effects on voltage-dependent electromechanical activity, Neurosci. Lett. 404 (2006) 270–275.
[9] L. Rajagopalan, N. Patel, S. Madabushi, J.A. Goddard, V. Anjan, F. Lin, C. Shope, B. Farrell, O. Lichtarge, A.L. Davidson, W.E. Brownell, F.A. Pereira, Essential helix interactions in the anion transporter domain of prestin revealed by evolutionary trace analysis, J. Neurosci. 26 (49) (2006) 12727–12734.
[10] K. Matsuda, J. Zheng, G.G. Du, N. Klöcker, L.D. Madison, P. Dallos, N-linked glycosylation sites of the motor protein prestin: effects on membrane targeting and electrophysiological function, J. Neurochem. 89 (2004) 928–938.
[11] L. Deák, J. Zheng, A. Orem, G.G. Du, S. Aguiñaga, K. Matsuda, P. Dallos, Effects of cyclic nucleotides on the function of prestin, J. Physiol. 563 (2005) 483–496.
[12] K. Mio, Y. Kubo, T. Ogura, T. Yamamoto, F. Arisaka, C. Sato, The motor protein prestin is a bullet-shaped molecule with inner cavities, J. Biol. Chem. 283 (2007) 1137–1145.
[13] M. Murakoshi, K. Iida, S. Kumano, H. Wada, Immune atomic force microscopy of prestin-transfected CHO cells using quantum dots, Pflugers Arch. 457 (2009) 885–898.
[14] M.A. Larkin, G. Blackshields, N.P. Brown, R. Chenna, P.A. McGettigan, H. McWilliam, F. Valentin, I.M. Wallace, A. Wilm, R. Lopez, J.D. Thompson, T.J. Gibson, D.G. Higgins, Clustal W and Clustal X version 2.0, Bioinformatics 23 (2007) 2947–2948.

[15] K. Iida, K. Tsumoto, K. Ikeda, I. Kumagai, T. Kobayashi, H. Wada, Construction of an expression system for the motor protein prestin in Chinese hamster ovary cells, Hear. Res. 205 (2005) 262–270.
[16] D.Z.Z. He, B.N. Evans, P. Dallos, First appearance and development of electromotility in neonatal gerbil outer hair cells, Hear. Res. 78 (1994) 77–90.
[17] P. Dallos, N.E. Evans, R. Hallworth, Nature of the motor element in electrokinetic shape changes of cochlear outer hair cells, Nature 350 (1991) 155–157.
[18] D. Oliver, D.Z.Z. He, N. Klöcker, J. Ludwig, U. Schulte, S. Waldegger, J.P. Ruppersberg, P. Dallos, B. Fakler, Intracellular anions as the voltage sensor of prestin, the outer hair cell motor protein, Science 292 (2001) 2340–2343.
[19] S. Komatsu, K. Miyazaki, R.A. Tuft, M. Ikebe, Translocation of telokin by cGMP signaling in smooth muscle cells, Am. J. Physiol. Cell Physiol. 283 (2002) C752–C761.

Pflugers Arch - Eur J Physiol (2009) 457:885–898
DOI 10.1007/s00424-008-0560-z

SENSORY PHYSIOLOGY

Immune atomic force microscopy of prestin-transfected CHO cells using quantum dots

Michio Murakoshi · Koji Iida · Shun Kumano · Hiroshi Wada

Received: 22 April 2008 / Revised: 7 July 2008 / Accepted: 14 July 2008 / Published online: 2 August 2008

Abstract Prestin, a membrane protein of the outer hair cells (OHCs), is known to be the motor which drives OHC somatic electromotility. Electron microscopic studies showed the lateral membrane of the OHCs to be densely covered with 10-nm particles, they being believed to be a motor protein. Imaging by atomic force microscopy (AFM) of prestin-transfected Chinese hamster ovary (CHO) cells revealed 8- to 12-nm particle-like structures to possibly be prestin. However, since there are many kinds of intrinsic membrane proteins other than prestin in the plasma membranes of OHCs and CHO cells, it was impossible to clarify which structures observed in such membranes were prestin. In the present study, an experimental approach combining AFM with quantum dots (Qdots), used as topographic surface markers, was carried out to detect individual prestin molecules. The inside-out plasma membranes were isolated from the prestin-transfected and untransfected CHO cells. Such membranes were then incubated with antiprestin primary antibodies and Qdot-conjugated secondary antibodies. Fluorescence labeling of the prestin-transfected CHO cells but not of the untransfected CHO cells was confirmed. The membranes were subsequently scanned by AFM, and Qdots were clearly seen in the prestin-transfected CHO cells. Ring-like structures, each with four peaks and one valley at its center, were observed in the vicinity of the Qdots, suggesting that these structures are prestin expressed in the plasma membranes of the prestin-transfected CHO cells.

M. Murakoshi · K. Iida · S. Kumano · H. Wada (✉)
Department of Bioengineering and Robotics, Tohoku University,
6-6-01 Aoba-yama,
Sendai 980-8579, Japan
e-mail: wada@cc.mech.tohoku.ac.jp

Keywords Auditory system · Cochlea · Hair cell · Membrane · Motor systems · Imaging · Microscopy

Introduction

The high sensitivity, sharp frequency selectivity, and wide dynamic range of mammalian hearing are achieved by cochlear amplification, the mechanism of which is realized due to outer hair cell (OHC) somatic motility [1–4], operating at up to microsecond rates [5]. This motility was thought to be associated with a membrane protein in the lateral wall of OHCs [6], but was later found to be realized by the motor protein prestin [7].

Prestin consists of 744 amino acid residues with a molecular weight of around 81.4 kDa. Hydrophobicity analysis indicated that prestin has two large protruding fragments, i.e., N (approximately 100 amino acids [a.a.]) and C termini (approximately 250 a.a.), extending into the cytoplasm and a hydrophobic center core (approximately 400 a.a.) with 12 transmembrane domains [8]. Later, however, it was clarified that two of these domains do not penetrate the plasma membrane [9]. On the other hand, a prestin topology with 10 transmembrane domains has also been reported [10]. Among these termini, the STAS (after sulfate transporter and antisigma factor antagonist) domain (amino acids 525–713; molecular weight of 21 kDa), located at the C terminus of prestin [5], possibly occupies a large portion of the conformational space of the cytoplasmic region. Homooligomerization of prestin has been reported to be a tetramer [11, 12] and its N terminus is possibly important for this conformation [10].

Previous morphological studies of OHCs using an electron microscope have shown the lateral membrane of the OHCs to be densely covered with particles about 10 nm

in diameter, these particles being believed to be a motor protein [13–16]. The lateral membrane has also been observed by atomic force microscopy (AFM) and the existence of many particles with diameters of about 10 nm has also been reported [17]. Imaging by AFM of prestin-transfected Chinese hamster ovary (CHO) cells has revealed that particle-like structures 8–12 nm in diameter are possibly prestin [18]. However, since there are many kinds of intrinsic membrane proteins other than prestin in the plasma membranes of OHCs and CHO cells, it was impossible to clarify which structures observed in such membranes were prestin. More recently, prestin has been reported to be expressed in insect cells and has been purified from these cells. Using such purified prestin, its 3-D structure was clarified to be a bullet-shaped particle by transmission electron microscopy (TEM) [12]. However, the structure of purified prestin is not necessarily identical to that of prestin expressed in the native cell plasma membrane. In addition, TEM-based analysis of the protein structure requires time-consuming and cumbersome techniques for sample preparation to obtain a sufficient amount of purified protein for experimentation.

In the present study, an experimental approach combining AFM with quantum dots (Qdots), used as topographic surface markers, was employed to detect individual prestin molecules. The inside-out plasma membranes were isolated from the prestin-transfected and untransfected CHO cells. Such membranes were then incubated with antiprestin primary antibodies and Qdot-conjugated secondary antibodies. The plasma membranes of both types of CHO cells were subsequently observed by fluorescence microscopy and then scanned by AFM.

Materials and methods

Cells and cell culture

Prestin-transfected and untransfected CHO cells were used. The prestin-transfected CHO cells were constructed by transfection of gerbil prestin cDNA into CHO cells using pIRES-hrGFP-1a mammalian expression vectors (Stratagene, La Jolla, CA, USA). Those expression vectors contain humanized *Renilla reniformis* green fluorescent protein (hrGFP) gene and the GFP is expressed in the cytoplasm of the cells. CHO cell lines, which stably express prestin, were established using transfected cells by limiting dilution cloning. The expression and activity of prestin in the generated CHO cell lines were confirmed by immunofluorescence and whole-cell patch clamp measurements [19, 20]. CHO cells, which were not subjected to any transfection procedure, were used as the untransfected CHO cells.

The prestin-transfected and untransfected CHO cells were cultured in RPMI-1640 medium with 10% fetal bovine serum, 100 U penicillin/ml, and 100 μg streptomycin/ml at 37°C with 5% CO_2. At the beginning of every experimental procedure, the GFP fluorescence of the prestin-transfected CHO cells were observed by using a confocal laser scanning microscope (FV500, Olympus, Tokyo, Japan) equipped with a UPlan Apo ×20 (NA=0.70) objective and an Ar laser (488 nm) to confirm the expression of prestin.

Isolation of plasma membranes

The inside-out plasma membranes, i.e., cytoplasmic face is up, were isolated from the prestin-transfected CHO cells as described elsewhere [21]. The culture medium was removed and the cells were detached from a flask by incubation with 100 μM ethylenediamine tetraacetic acid (EDTA) in phosphate buffered saline (PBS) solution for 5 min at 37°C. The EDTA–PBS solution containing the cells was put into a tube and centrifuged at 250×*g* for 5 min. The supernatant was then removed and the culture medium was put into the tube. The culture medium containing the cells was agitated by pipetting in that tube and deposited on glass-bottomed dishes (Asahi Techno Glass, Chiba, Japan). After overnight culture, most of the cells had become reattached and spindle-shaped on the substrate. The culture medium was discarded and the cells were washed twice with an external solution (145 mM NaCl, 5.8 mM KCl, 1.3 mM $CaCl_2$, 0.9 mM $MgCl_2$, 10 mM HEPES, 0.7 mM Na_2HPO_4, and 5.6 mM glucose; pH 7.3) warmed to 37°C for removal of unwanted materials, such as cell fragments and proteins contained in the culture medium attached to the surfaces of the cells and substrate. The dish was immersed for 3 min in a hypotonic buffer (10 mM piperazine-*N*,*N*′-bis(2-ethanesulfonic acid), 10 mM $MgCl_2$, 0.5 mM ethylene glycol bis(2-aminoethyl ether)-*N*,*N*,*N*′,*N*′-tetraacetic acid; pH 7.2), which had been cooled to 4°C. The cells were then sheared open by gentle exposure to a stream of the hypotonic buffer using a 1-ml pipette (Gilson, Villiers, France) several times, resulting in the isolation of the inside-out basal plasma membranes. After the isolated plasma membranes had been washed with PBS three times, they were incubated with a high-salt buffer (2 M NaCl, 2.7 mM KCl, 1.5 mM KH_2PO_4, 1 mM Na_2HPO_4; pH 7.2) for 30 min at room temperature to remove the cytoskeletal materials and the peripheral proteins [22]. The isolated membranes were then incubated with 0.05% trypsin for 1 min at room temperature to remove the remaining materials.

Sample preparation for prestin labeling with Qdots and AFM imaging

The isolated plasma membranes were fixed with 4% paraformaldehyde in PBS for 30 min at room temperature.

After fixation, the membranes were rinsed three times with PBS and incubated with Block Ace (Dainippon Pharmaceutical, Osaka, Japan) for 30 min at 37°C. After PBS washing, the membranes were incubated with goat antiprestin N terminus primary antibody (Santa Cruz Biotechnology, Santa Cruz, CA, USA) at a dilution of 1:100 in PBS overnight at 4°C. The membranes were then washed with PBS and incubated with Qdot® 655-conjugated rabbit antigoat IgG secondary antibody (Invitrogen, Carlsbad, CA, USA) at a dilution of 1:200 in PBS for 60 min at 37°C. Finally, the membranes were washed with Hanks' balanced salt solution (HBSS; 5.33 mM KCl, 0.44 mM KH_2PO_4, 137.93 mM NaCl, 0.34 mM Na_2HPO_4, 0.56 mM glucose; pH 7.3) and immersed in this solution filtered with a 0.22-μm pore-size syringe filter (Millipore, Billerica, MA, USA).

Fluorescence microscopy

Fluorescence images were obtained from the isolated membranes of the prestin-transfected CHO cells and those of the untransfected CHO cells by an inverted fluorescence microscope equipped with a Plan Apo ×100 (NA=1.40) oil immersion objective and a cooled CCD camera (DP70, Olympus), which comprised a part of the AFM used in this study, the exposure time being 2 s. This system enables simultaneous recording of fluorescence and AFM images of the same sample. A mercury lamp was used as a light source. Qdot fluorescence was detected with a wide-band filter cube (U-MWIG, Olympus) composed of a 520- to 550-nm excitation filter, a 565-nm dichroic mirror, and a 580-nm emission filter.

Atomic force microscopy

An AFM (NVB100, Olympus), in which the AFM unit is mounted on an inverted fluorescence microscope (IX70, Olympus), was used, such mounting making it easy to position the tip above the cells. This AFM is controlled by NanoScope IIIa (Digital Instruments, Santa Barbara, CA, USA; software version, v4.23). A V-shaped silicon nitride cantilever (OMCL-TR400PSA-2, Olympus) with a spring constant of 0.02 N/m was used. The cantilever has a pyramidal tip, the typical radius of its curvature being 16± 1 nm (personal communication with Olympus). To minimize sample damage during scanning, AFM images were obtained using the oscillation imaging mode (Tapping mode™, Digital Instruments). The cantilever was oscillated near its resonance frequency in liquid (3.6–4.7 kHz). Low- (60.0×60.0 μm), middle- (11.7×11.7 μm), and high-magnification images (2.3×2.3 μm) were obtained at a scan rate of 1.0 Hz, i.e., the scan speeds were 120, 23.4, and 4.6 μm/s, respectively. By scanning the sample with this mode, the height and phase images of the sample surface were obtained. The phase image was constructed by monitoring the phase lag between the input signal to the cantilever (i.e., driving signal used to drive the cantilever at its resonance for tapping mode, a sinusoidal signal of 3.6–4.7 kHz in this study) and the output signal from the cantilever detected by the laser system of the AFM (i.e., detected signal from the photodiode detector). For all AFM images, the samples were scanned from left to right. Each scan line had 512 points of data and an image consisted of 512 scan lines.

Analysis of AFM images

The original AFM images were flattened by use of a software program (NanoScope v4.23, Digital Instruments) to eliminate background slopes and to correct dispersions of individual scanning lines. AFM images were generated by raster scanning with a cantilever across a sample, i.e., left to right and top to bottom in a zigzag pattern. During this scanning, the topological data were continuously obtained in the transversal direction of the AFM image, i.e., left to right of the image, while such data in the longitudinal direction, i.e., top to down of the image, were intermittent. Thus, the topological data in the transversal direction of the image were more reliable than those in the longitudinal direction. The transversal sizes of the observed structures were, therefore, measured.

In the present study, Qdots were used as topographic surface markers. As the prestin molecules were labeled with primary and secondary antibodies, the distance between a Qdot and a prestin molecule was estimated to be approximately 20 nm [23]. The primary antibody used in this study reacts with the cytoplasmic N terminus of prestin. Since such terminus consists of approximately 100 a.a., its length was estimated to be approximately 31 nm [24]. Assuming that the antibody binds to the tip of the N terminus, the estimated maximum distance between a Qdot and the transmembrane domain of a prestin molecule is approximately 50 nm. Due to the architecture of the AFM system used in the present study, a 133-nm square AFM image containing one Qdot at its center was obtained by applying cubic spline interpolation to a high-magnification AFM image. All structures observed within 66.5 nm apart from the center of the Qdot were subjected to subsequent size analysis.

The diameter of the observed structure was estimated using a simple geometric model since such sizes are prone to overestimation due to the radius of the curvature of the AFM tip [25]. The relationship between the diameter of the structure observed by the AFM (2Δ) and its actual diameter ($2r$) is given by:

$$2\Delta = 2\left\{(R+r)^2-(R+H/2)^2\right\}^{1/2} \quad (1)$$

where R is the radius of the curvature of the AFM tip and H is the thickness of the plasma membrane, as described in